COMMUNICATION

Long-term photostability in Terephthalate Metal Organic Frameworks

Diego Mateo,[a] Andrea Santiago-Portillo,[b] Josep Albero,[a] Sergio Navalón,[b] Mercedes Alvaro[b] and Hermenegildo García*[a]

Abstract: Prolonged (weeks) UV-Vis irradiation under Ar of UiO-66(Zr), UiO66 Zr-NO₂, MIL101 Fe, MIL125 Ti-NH₂, MIL101 Cr and MIL101 Cr(Pt) shows that these MOFs undergo photodecarboxylation of benzenedicarboxylate (BDC) linker in a significant percentage depending on the structure and composition of the material. Routine characterization techniques such as XRD, UV-Vis spectroscopy and TGA fail to detect changes in the material, although porosity and surface area change upon irradiation of powders. In contrast to BCD containing MOFs, zeolitic imidazolate ZIF-8 does not evolve CO_2 or any other gas upon irradiation.

Due to a combination of positive features including flexibility in the design, wide selection of metals and organic linkers, possibility to incorporate co-catalysts and large surface area, metal organic frameworks (MOFs) are currently attracting considerable attention as photocatalysts to perform degradation of organic pollutants and for production of solar fuels.[1, 2]

In one possible general photochemical pathway, light absorption by the organic linker generates a localized excited state that decays transferring one electron to the metal node.[2] The favorable orbital overlap of organic linkers and metal nodes due to the spatial arrangement of the crystal lattice and the strong Coulombic and coordinative bonds is favorable upon photoexcitation for the occurrence of a fast and efficient generation of a charge separated state able to promote reductions and oxidation reactions.[3, 4] Particularly, in the context of solar fuel production, the combination of suitable amino substituted organic linkers and mixed metal nodes has resulted in photocatalysts with notable activities that could be further improved in the coming years by adequate MOF design.[2, 5-7] One particular case where MOFs have shown promising photocatalytic activity is for the photocatalytic CO_2 reduction upon solar light irradiation.[8-11] Photocatalytic solar light utilization could be one of the possible key processes to develop sunlight-based renewable energy in the future, leading to a decrease of atmospheric CO_2 emissions.[2, 12, 13]

One of the prerequisites for an efficient photocatalyst is stability under irradiation conditions, since otherwise its activity would decrease over the time due to decomposition of the photocatalytic sites. There is a vast number of reports stating that the MOFs used as photocatalysts are stable under irradiation conditions,

including those based on benzenedicarboxylate (BDC).[8, 14, 15] However, this conclusion is frequently based on relatively short time experiments, typically of only a few hours and characterization of the used material by X-ray diffraction (XRD). As it will be shown latter, XRD can, however, be misleading since crystallinity of the residual material may not report on ligand decomposition.

For their use as photocatalysts, photochemical stability is a prerequisite that has to be confirmed on solid ground, particularly considering the photochemical reactivity of a large number of organic compounds and functional groups.[16] Since several of the most efficient MOFs in photocatalysis, such as UiO-66 ((UiO: University of Oslo), MIL-101 (MIL= Matériaux de l'Institut Lavoisier) and MIL-125, contain aromatic carboxylates as linkers and some compounds of this class have been reported to be photolabile,[17] [18-21] it is worth to address specifically the photostability for MOFs containing aromatic polycarboxylates for long irradiation periods, characterizing the materials by a combination of techniques.

The present study reports long term (weeks) irradiation of some of the MOFs most frequently reported as photocatalysts that contain BDC linkers. Evolution of significant proportions of CO_2 from these MOFs upon UV-Vis irradiation is observed here, regardless the nature of substituents on the BDC linkers (such as -NO_2 or NH_2) or the presence of metal nanoparticles (Pt) as guests. It will be shown that, while no changes can be detected by XRD of MOF materials irradiated for weeks and surface area measurements may show only minor differences, analysis of the gas phase shows for BDC MOFs gas evolution in an extent that clearly depends on the nature of the MOF. It has been observed that BDC can exhibit distinctive stability depending on the composition and structure of the MOF. These results have been rationalized based on homogeneous phase photodecomposition of terephthalate and clearly demonstrates that the long-term (days/weeks) photostability of MOF photocatalysts depends on their structure and cannot be determined from irradiation experiments lasting only a few hours.

Zirconium(IV)-carboxylate based MOFs, exhibiting different topologies, pore size and containing different functional groups, have been widely described as photocatalysts for different reactions, including H_2 generation on Pt-containing samples[22] and the photocatalytic decolorization of methylene blue on Ti-exchanged sample,[22, 23] to name a few. The strong coordinative bonds between the Zr(IV) ions and carboxylate oxygens in closed packed structure confer to UiO66 Zr an improved chemical, mechanical and thermal stability compared to other MOFs containing metal ions with lesser electrostatic charge, such as MOF-5 (Zn^{2+}), HKUST-1 (Cu^{2+}) or even MIL-88 (Cr^{3+}).[24] The structure of UiO66 Zr with empirical formula $Zr_6O_4(OH)_4(BDC)_6$ comprises $Zr_6O_4(OH)_4$ octahedra that are 12-fold connected to adjacent octahedra through BCD linkers, resulting in a highly packed fcc structure. The strong Zr-O bonds formed between the cluster and carboxylate ligands and the ability of the inner Zr_6-cluster to rearrange reversibly upon removal or addition of μ_3-OH groups without changes are thought to contribute to the increased stability of UiO66 Zr and others related Zr MOF (i.e. UiO-67). Indeed, they have been reported among the most stable MOFs in

[a] Dr. D. Mateo, Dr. J. Albero and Prof. H. García
Instituto Universitario de Tecnología Química CSIC-UPV
Universitat Politècnica de València
Av. De los Naranjos s/n, 46022, València, Spain.
E-mail: hgarcia@qim.upv.es
[b] Dr. A. Santiago-Portillo, Dr. S. Navalón and Prof. M. Alvaro
Departamento de Química,
Universitat Politècnica de València
Camino de Vera s/n, 46022, València, Spain.

Supporting information for this article is given via a link at the end of the document.

the literature.[24, 25] In the present case, UiO66 Zr MOF was prepared following a reported procedure that results in UiO66 Zr samples with high crystallinity and low defect density (see preparation procedure in supplementary information), and submitted this material to prolonged photochemical irradiation in order to test its stability. In these experiments, UiO66 Zr (100 mg, 0.71 mmol of carboxylate groups) as fine powder was previously outgassed at 150 °C for 12 h in a quartz reactor and, afterwards, purged for 15 min with Ar prior to irradiation, to exclude the presence of oxygen and moisture. The sample was exposed to UV-Vis light from a 300 W Xe lamp (100 mW×cm^{-2}). The temperature of the irradiation was maintained during the experiment at 25 °C. The atmosphere of the reactor was continuously analyzed in order to determine gas evolution from the solid upon continuous UV-Vis illumination for several days. Analyses were performed with a MicroGC equipped with two columns, a MolSieve 5A monitoring H_2 or O_2 evolution and a Pore Plot Q column for detection of CO_2, CO and up to C4 hydrocarbons. The only photoproduct detected in the gas phase in most of the cases was CO_2. Figure 1 shows the temporal CO_2 evolution upon continuous irradiation of powdered UiO66 Zr for 19 days under Ar atmosphere.
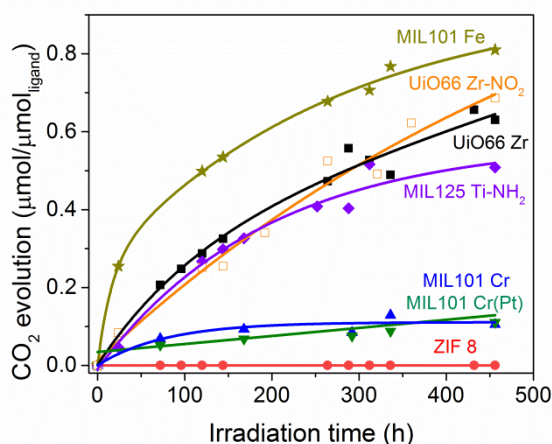

Figure 1. Temporal profiles of CO_2 evolution from the different MOFs under study: UiO66 Zr (black squares), UiO66 Zr-NO_2 (orange empty squares), MIL101 Fe (dark yellow stars), Mil125 Ti-NH_2 (purple diamonds), MIL101 Cr (blue triangles), MIL101 Cr-Pt (green inverted triangles) and ZIF-8 (red dots), normalized to the ligand amount (expressed in µmol). Reaction conditions: continuous UV-Vis irradiation by a 300 W Xe lamp for 456 h (19 days) under Ar atmosphere. Lines show data point trends.

As can be observed in Figure 1, upon UV-Vis irradiation a continued evolution over 19 days of CO_2 was observed for UiO66 Zr. Note that the presence of other gases such as CO, H_2 or CH_4, if formed, was under the detection limit in these experiments (0.5 µmol/mg). The origin of the evolved CO_2 is most probably photodecarboxylation of the BDC linkers. Photodecarboxylation is a process that has been previously reported for phenylacetic acid and other carboxylic acid-containing aromatic compounds.[17-19] The presence of –NO_2 or –NH_2 as substituents in the BDC linker has been used to tune the optoelectronic properties of MOFs. In this regard, UiO66 Zr-NO_2 (see preparation procedure in supplementary information) was also submitted to prolonged irradiation under identical conditions as UiO66 Zr. As can be observed in Figure 1, similar temporal evolution of CO_2 as that of UiO66 Zr was observed for UiO66 Zr-NO_2, the presence of NO_2 groups on the linkers not altering significantly the photodecarboxylation rate of the BDC ligands.

In a similar way, MIL101 Cr, MIL101 Fe and MIL125 Ti-NH_2 MOFs with high crystallinity were prepared following reported

procedures[26] (see supplementary information) and submitted to UV-Vis light irradiation after thermal outgassing as powders in the absence of oxygen and moisture. The empirical formula of MIL100 Fe is $Fe_3OCl(H_2O)_2(BDC)_3$, where the nodes are constituted by three octahedra sharing a μ_3-O corner and having one Fe^{3+} ion at the center. Each Fe_3-μ-O node is connected to six BDC linkers with additional Cl^- or H_2O ligands occupying the remaining three coordination sites.[27] The MIL101 Cr empirical formula is $Cr_3F(H_2O)_2O(BDC)_3 \cdot nH_2O$ and is isostructural with MIL Fe replacing Fe^{3+} by Cr^{3+} ions and having F^- instead of Cl^- as charge compensating ion. MIL101 lattice defines a zeotype cubic structure with ~30 Å pore size and ~2000 m^2/g surface area.[28] Finally, the empirical formula of MIL125 Ti-NH_2 is $[Ti_8O_8(OH)_4(C_6H_3C_2O_4NH_2)_6]$. MIL125 Ti-$NH_2$ structure is formed by cyclic octamers constituted from corner or edge sharing octahedral titanium units. These octamers are connected to 12 other cyclic octamers through BDC linkers, leading to a porous quasi-cubic tetragonal structure.[29]

As can be observed in Figure 1, CO_2 evolution as the only detectable product in the gas phase was also observed over the time upon prolonged UV-Vis irradiation of MIL101 Fe, MIL125 Ti-NH_2 and MIL101 Cr. The MIL101 Fe exhibits the highest CO_2 evolution normalized to the amount of ligand. In contrast, CO_2 evolution upon irradiation of MIL101 Cr is about six times smaller than that of MIL101 Fe under the same conditions, in spite that both MOFs have BDC as common organic linker and the same structure. This fact illustrates the notable influence on the photodecarboxylation rate of the metal and the precise orbital energy alignment of the metal nodes and the linker. Thus, more efficient ligand-to-metal charge transfer in the case of MIL101 Cr in comparison with MIL101 Fe would quench more efficiently the localized BDC excited state decreasing the photodecarboxylation rate. For comparison purposes MIL101 Cr containing 1 wt% Pt nanoparticles (MIL101 Cr(Pt)) was also submitted to identical irradiation conditions, observing very similar temporal evolution as that of MIL101 Cr. It could be expected that the presence of Pt nanoparticles influences the photoinduced charge transfer in this MOF, and thus the photodecarboxylation rate. Nevertheless, it seems that the presence of the Pt nanoparticles, a universal co-catalyst in the photocatalytic H_2 evolution, does not play a role in the photodecarboxylation. The temporal profile of CO_2 evolution for MIL101 Cr and MIL101 Cr(Pt) exhibits also some differences respect to that of UiO66 Zr and MIL101 Fe, since most of the CO_2 evolves in the first 100 h of irradiation and, after this initial period, CO_2 evolution is remarkably slower. This experimental observation could be interpreted considering that the population of BDC linkers that undergo faster decarboxylation are those located at structural defects. The use of MOFs containing defective structures has been reported as an effective method to enhance the photocatalytic activity of these materials[30]. These defects could act as recombination centers, inhibiting further photodecarboxylation.

MIL125 Ti-NH_2 is also among the most studied MOFs in photocatalysis.[29] MIL125 Ti-NH_2 was also submitted to prolonged UV-Vis irradiation for 19 days (Figure 1). Again, CO_2 evolution was observed. Note that, in spite that UiO66, MIL101 and MIL125 MOFs have all BDC as organic linkers the photodecarboxylation profiles are notably different as consequence of the different electronic properties.

Control experiments in dark conditions were carried out in order to confirm that the decarboxylation process in the studied MOFs is induced by light. In these experiments, the MOFs were outgassed and submitted to the irradiation conditions although the photoreactor was covered with opaque aluminum foil, while light irradiation from the 300 W Xe lamp was kept for 19 consecutive days. Measurement of the gases evolved during this period did not detect CO_2 or any other gas for any of the samples under

study. This negative result confirms that light exposure is the origin of CO_2 evolution, excluding dark-aging effects.

Besides BDC containing MOFs and for comparison purposes, the behavior of ZIF-8 (Zeolitic Imidazole Framework) MOF under the same conditions was also studied. ZIF-8 is composed by Zn^{2+} ions tetrahedrally coordinated by four imidazolate rings with unit formula $Zn_6(mIm)_{12}$ (mIm= 2-methylimidazolate). The structure contains one central nanopore per unit cell, with 2500 $Å^3$ volume and 11.6 Å pore diameter.[31] ZIF MOF series containing imidazole based linkers has been widely used in different fields due to their robust structure, resistance to thermal changes and chemical stability.[32, 33] As can be observed in Figure 1 and in contrast to the previous MOFs containing BDC, ZIF-8 did not present evolution of any detectable gas, including CO_2, upon continuous UV-Vis irradiation for 19 days under Ar atmosphere. This result agrees with carboxylate as the origin of CO_2.

An estimation of the percentage of carboxylate groups decomposed during irradiation from BDC-containing MOFs can be obtained from CO_2 quantification, considering the MOFs mass exposed and its empiric formula. The maximum amount of CO_2 per MOF mass at final reaction time (19 days), corresponded to 40 % of the BDC carboxylate groups present in the MIL101 Fe sample submitted to irradiation. While UiO66 Zr and UiO66 Zr-NO_2 showed decarboxylation percentage over 30 %. In a similar way, it was estimated that only 5 % of the total carboxylate groups in the exposed MIL101 Cr and MIL101 Cr(Pt) MOFs were decomposed to CO_2, while a 28 % was found for the MIL125 Ti-NH_2. A summary of the percentages of carboxylate groups decomposed from BDC linkers during irradiation is presented in Table 1.

Aimed at determining if routine characterization techniques can reveal changes at this remarkable CO_2 evolution level, the samples exposed to photodecarboxylation were characterized by XRD, BET and UV-Vis spectroscopy. Analogous data for the samples treated in the dark are provided in the supplementary information as Figures SI6, SI7 and Table SI1. As expected in view of the absence of CO_2 evolution and the known stability, no changes in XRD, surface area, pore volume, pore size and UV-Vis absorption spectra were found for the samples in the dark.

Regarding the samples submitted to prolonged irradiation, it was anticipated that the decomposition of one in every 2.5-3 carboxylate groups would be reflected in the MOF crystalline structure. However, XRD patterns of the long-term irradiated samples exhibit minor changes in the position and relative intensity respect to the fresh samples. Figure 2 presents the XRD patterns of fresh and irradiated samples for UiO66 Zr, MIL101 Fe, MIL125 Ti-NH_2 and ZIF-8 and those others of UiO66 Zr-NO_2, MIL101 Cr, MIL101 Cr(Pt) are collected in Figure S2 in supplementary Information. As commented in the introduction, the lack of variation in the XRD patterns is generally considered as an evidence in support of stability in photocatalytic tests of a few hours' time. However, as illustrated by Figures 2 and S2, this characterization can miss decarboxylation in a large percentage and caution should be taken when interpreting the lack of important XRD changes.

In the present study, the most remarkable changes in the XRD patterns were variations on the relative intensity of the small-angle peaks, clearly noted for MIL-101. Apparently, removal of one third or more of the carboxylic acids in the linkers is not sufficient to promote a substantial collapse of the MOF structure. Thus, the creation of structural defects will be mostly undetected by the XRD analysis. It is proposed, however, that generation of defects is the reason of the change in the small-angle relative intensity peaks in the case of MIL-101.
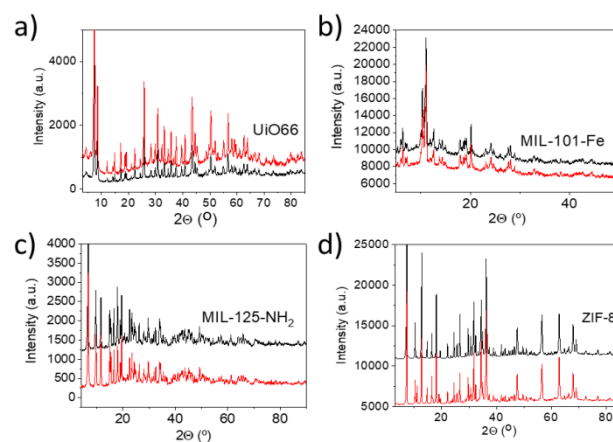

Figure 2. XRD patterns of UiO66 Zr (a), MIL101 Fe (b), MIL125 Ti-NH_2 (c) and ZIF-8 (d) pristine (red) and irradiated (black) for 456 h with a 300 W Xe lamp under Ar atmosphere.

To search for the generation of defects, the textural properties of these MOFs after extended irradiation were also analyzed and compared to those of the fresh samples. Thus, the BET surface area and pore volume and size for pristine and irradiated MOFs were measured and the results are summarized in Table 1, while Supplementary Information indicates the conditions of the measurements and presents the corresponding adsorption isotherms. Note that the irradiations were carried out on thermally activated, dry powders, without any solvent or substrate and, therefore, the presence of impurities blocking the pores, others than those generated from the linkers should not be expected.

The BET surface area of all the irradiated UiO66 Zr, UiO66 Zr-NO_2, MIL125 Ti-NH_2, MIL101 Cr and MIL101 Cr(Pt) samples decreased after prolonged light irradiation for 19 days as can be seen in Table 1. Only in the case of ZIF-8 that does not undergo decarboxylation, a slight increase of the specific surface area after extended light irradiation was measured. It is worth noticing that the BET surface of MIL101 Fe presented only minor changes in spite that this sample has undergone the highest photodecarboxylation percentage in the series. Thus, it seems that, as in the case of XRD, also variations in BET surface area are not linearly correlated with the photodecomposition.

Similarly, variations of the pore size are not directly related to the occurrence of photodecarboxylation. Thus, for the irradiated UiO66 Zr, UiO66 Zr-NO_2, MIL125 Ti-NH_2 and ZIF-8 samples the pore size increased a 45.6, 4.0, 12.7 and 28.4 %, respectively, while, on the contrary, MIL101 Fe after a large percentage of decarboxylation decreases the pore size reduction by 76.2 %. The pore size of the irradiated MIL101 Cr and MIL101 Cr(Pt) remained practically unchanged. Again, no direct correlation between pore volume variation after irradiation and the degree of photodecarboxylation can be inferred.

From adsorption data it can be concluded that porosity of MOFs are modified by photodecarboxylation, although in different extent depending on composition and structure, there being difficult to correlate directly porosity changes and photostability. For instance, MIL101 Fe, which is the sample with the highest CO_2 evolution per µmol of ligand suffered minor changes in BET surface area, although its pore volume and size have been drastically reduced. In contrast, UiO66 Zr, which has also shown a notable CO_2 evolution upon irradiation, presents a decrease in BET surface area while the pore volume and size have increased.

Thermogravimetric analysis (TGA) of pristine and long-term irradiated MOFs were also carried out in order to determine possible changes in thermal stability caused by BDC decarboxylation. The results are presented in Figure S4. As it can

be seen there, no significant changes can be found between pristine and long-term irradiated MOFs.

The diffuse reflectance UV-Vis absorption spectra of the pristine MOFs and after light exposure were also recorded. The UV-Vis results are presented Figure S5 in supplementary information. As it can be observed there, the diffuse reflectance UV-Vis absorption spectra of all the samples remained practically unchanged after 19 days of continuous light irradiation.

Thus, none of the above characterization data are adequate to address photostability issues in BDC-containing MOFs. It is proposed that the result of photodecarboxylation should be the creation of defects with no much structural change.

Table 1. Summary of the BET surface area, pore volume and size for pristine and irradiated samples of UiO66 Zr, UiO66 Zr-NO$_2$, MIL101 Fe, MIL125 Ti-NH$_2$, MIL101 Cr, MIL101 Cr(Pt) and ZIF-8 for 456 h under Ar atmosphere with a 300 W Xe lamp, as well as the percentage of decarboxylated groups.

Sample	Area BET (m^2/g)	Pore Volume (cm^3/g)	Pore Size (Å)	% of decarboxylated ligands
UiO66 Zr	857.3	0.74	34.76	
				31%
UiO66 Zr irradiated	711.5	0.9	50.6	
ZIF-8	720.53	0.38	21.09	
				0%
ZIF-8 irradiated	744.80	0.47	24.83	
MIL101 Cr	2369.83	2.01	33.93	
				5%
MIL101 Cr irradiated	2074.80	1.65	31.85	
MIL101 Cr(Pt)	3384.59	1.78	21.08	
				5%
MIL101 Cr(Pt) irradiated	3100.38	1.31	20.46	
MIL125 Ti-NH$_2$	1125.46	1.74	61.71	
				28%
MIL125 Ti-NH$_2$ irradiated	860.46	1.38	69.56	
MIL101 Fe	653.86	1.38	87.30	
				40%
MIL101 - Fe irradiated	645.58	0.34	20.82	
UiO66 Zr-NO$_2$	676.66	0.46	26.98	43%
UiO66 Zr-NO$_2$ irradiated	408.11	0.29	27.97	

In summary, continuous long-term irradiation of MOFs with different structures such as UiO66 Zr, UiO66 Zr-NO$_2$ MIL101 Cr, MIL101 Cr(Pt), MIL101 Fe and MIL125 Ti-NH$_2$ have shown a significant degree of CO$_2$ evolution as consequence of photodecarboxylation of the BDC linker, but this photochemical instability does not result in significant changes in XRD or UV-Vis absorption spectra, while the magnitude of the porosity change is difficult to correlate with the percentage of CO$_2$ evolution.

To gain further understanding in the origin of the photochemical CO$_2$ evolution, a photostability study in H$_2$O of BDC and a mixture of BDC and ZrCl$_4$ was carried out analyzing the gas evolution from the solution upon continuous irradiation under Ar atmosphere for 10 days. The aim of these experiments was to show the occurrence of photodecarboxylation of the organic linker regardless the absence or the presence of metal ions present in MOF nodes. Figure 3 summarizes the results obtained for a mixture of terephthalic acid and ZrCl$_4$ at the molar ratio corresponding to the UiO66 Zr formula. For comparison this Figure 3 also includes the results of 2-methylimidazole irradiation. It should be noted that although these controls show the intrinsic reactivity of BDC to undergo photodecarboxylation, it can be expected that the photodecarboxylation rate will depend on the available ligand excited state deactivation pathways and the nature of the metal ions involved, explaining in this way the differences in the temporal CO$_2$ evolution shown in Figure 1.
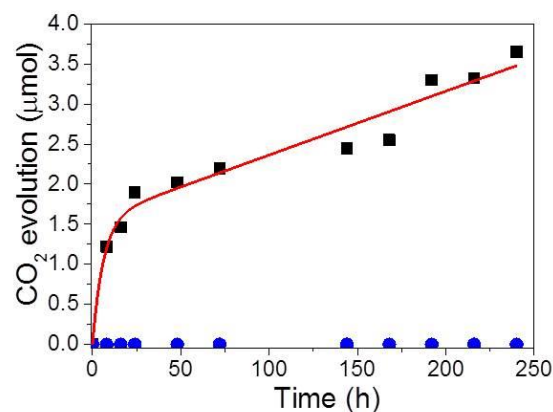

Figure 3. (a) CO$_2$ evolution from terephthalic acid (59 mg) and ZrCl$_4$ (88 mg) black squares, and 2-methylimidazole (60 mg) and Zn(NO$_3$)$_2$·6H$_2$O (167 mg) blue dots, solutions in H$_2$O (20 mL) under continuous irradiation with a 300 W Xe lamp for 10 days in Ar atmosphere. Red line indicates data point trend.

As can be observed in Figure 3, increasing amounts of CO$_2$ over the time were measured from the solution upon continuous light irradiation. The amount of CO$_2$ increased rapidly during the first day, then the CO$_2$ evolution was much lower during the measured 10 days. Observation of CO$_2$ evolution from the BDC/ZrCl$_4$ mixture lends support to the assumption that the origin of the CO$_2$ evolved upon irradiation of UiO66 Zr is photo decarboxylation of terephthalic acid. The final CO$_2$ amount measured in H$_2$O solution accounted for about 7 % of the total amount of carboxylate groups. Analysis of the liquid phase by reverse phase-chromatography using a photodiode array detector was also carried out, and a mixture of terephthalic and benzoic acids at about 95:5 ratio, respectively, was determined.

Solid-state ^{13}C NMR spectroscopy was carried out to UiO66 Zr after irradiation and compared with that of pristine UiO66 Zr. The spectra are presented as Figure 4. In addition, the solid-state ^{13}C

NMR of terephthalic acid as solid has been also measured, and the result is presented in the supplementary Information as Figure SI8. Peaks at 130, 132 and 173 ppm in terephthalic acid were assigned to carbons in the aromatic ring and the carbonyl groups, respectively.[34] Analogous peaks can be observed from pristine UiO66 Zr at 127, 136 and 169 ppm in accordance with the literature (Figure 4).[35] However, upon extended UiO66 Zr irradiation the peak at 127 ppm decreases in intensity and a new more intense peak appears at 130 ppms. The other two peaks also shift to lower field, particularly the carboxylate carbon that after irradiation is recorded less intense and broader at 172 ppm. The variation of the ^{13}C NMR spectra clearly correlates with the occurrence of the photodecarboxylation upon prolonged irradiation.
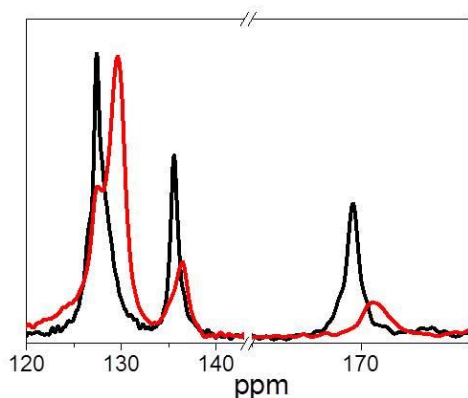

Figure 4. ^{13}C NMR spectra of pristine (black line) and irradiated UiO66 Zr MOF (red line).

2-Methylimidazole and $Zn(NO_3)_2$ mixture were also irradiated in H_2O under Ar atmosphere for 10 days. As noted earlier, no CO_2 was detected under these conditions (Figure 3). Moreover, after irradiation, the solution was analysed by ^1H and ^{13}C NMR spectroscopy, but no other compounds apart from the initial 2-methylimidazole were identified (Figure S9 in supplementary information).

In conclusion, the long-term photostability evaluation as powders of BDC-containing MOFs shows that, in contrast to the numerous reports in the field, they decompose evolving CO_2 in a significant percentage respect to the initial carboxylate content. The temporal CO_2 evolution depends on the composition and structure of the MOF, being markedly high for MIL101 Fe, UiO66 Zr or MIL125 Ti-NH₂, which are currently among the most used MOF in photocatalysis. The differences in photodecarboxylation rate reflects the influence of the node-linker interaction on the deactivation of the exciton localized on the linker. Interestingly, in spite of the large decarboxylation level that can be achieved, routine characterization techniques such as XRD, UV-Vis spectroscopy and TGA fail to report on this photochemical reaction, while adsorption measurements reveal changes that are difficult to correlate directly with the level of decarboxylation. Solid-state ^{13}C NMR spectroscopy is a suitable technique when the degree of photodecarboxylation is sufficiently high. Overall, the present experimental data shows that the widely assumed photostability tests for MOFs have to be revisited by conducting studies at long irradiation times and measuring gas evolution.

Experimental Section

The MOFs synthetic procedures are described in Supplementary Information. All MOF samples were degassed through activation at 150 ^0C overnight under vacuum prior irradiation. For the photodegradation tests, a certain amount of MOF sample was placed inside a quartz photoreactor equipped with cooling system. After purging the atmosphere with Ar, the MOF samples were irradiated with a 300 W Xe lamp. The gases evolved were analysed by a MicroGC equipped with two columns, a MolSieve 5A for H_2 or O_2 evolution and a Pore Plot Q column for CO_2, CO and up to C4 hydrocarbons. Further details are provided in Supplementary Information.

[1] R. N. Amador, M. Carboni, D. Meyer, *RSC Advances* **2017**, *7*, 195-200.
[2] A. Dhakshinamoorthy, A. M. Asiri, H. García, *Angewandte Chemie International Edition* **2016**, *55*, 5414-45.
[3] M. de Miguel, F. Ragon, T. Devic, C. Serre, P. Horcajada, H. García, *ChemPhysChem* **2012**, *13*, 3651-4.
[4] T. Tachikawa, J. R. Choi, M. Fujitsuka, T. Majima, *The Journal of Physical Chemistry C* **2008**, *112*, 14090-101.
[5] H. Wang, Q.-L. Zhu, R. Zou, Q. Xu, *Chem* **2017**, *2*, 52-80.
[6] S. Remiro-Buenamañana, M. Cabrero-Antonino, M. Martínez-Guanter, M. Álvaro, S. Navalón, H. García, *Applied Catalysis B: Environmental* **2019**, *254*, 677-84.
[7] Y. An, Y. Liu, P. An, J. Dong, B. Xu, Y. Dai, X. Qin, X. Zhang, M.-H. Whangbo, B. Huang, *Angewandte Chemie International Edition* **2017**, *56*, 3036-40.
[8] A. Dhakshinamoorthy, Z. Li, H. Garcia, *Chemical Society Reviews* **2018**, *47*, 8134-72.
[9] R. Li, W. Zhang, K. Zhou, *Advanced Materials* **2018**, *30*, 1705512.
[10] B. Han, X. Ou, Z. Deng, Y. Song, C. Tian, H. Deng, Y.-J. Xu, Z. Lin, *Angewandte Chemie International Edition* **2018**, *57*, 16811-5.
[11] J. Liu, Y.-Z. Fan, X. Li, Z. Wei, Y.-W. Xu, L. Zhang, C.-Y. Su, *Applied Catalysis B: Environmental* **2018**, *231*, 173-81.
[12] X. Kang, Q. Zhu, X. Sun, J. Hu, J. Zhang, Z. Liu, B. Han, *Chemical Science* **2016**, *7*, 266-73.
[13] D. Sun, Y. Gao, J. Fu, X. Zeng, Z. Chen, Z. Li, *Chemical Communications* **2015**, *51*, 2645-8.
[14] Y. Jing, J. Wang, B. Yu, J. Lun, Y. Cheng, B. Xiong, Q. Lei, Y. Yang, L. Chen, M. Zhao, *RSC Advances* **2017**, *7*, 42030-5.
[15] P. Wu, M. Jiang, Y. Li, Y. Liu, J. Wang, *Journal of Materials Chemistry A* **2017**, *5*, 7833-8.
[16] N. J. Turro, V. Ramamurthy, J. C. Scaiano, *Modern Molecular Photochemistry of Organic Molecules*, Viva Books, published by arrangement with University Science Books …, **2017**.
[17] D. Budac, P. Wan, *Journal of Photochemistry and Photobiology A: Chemistry* **1992**, *67*, 135-66.
[18] C. P. Joshua, G. E. Lewis, *Tetrahedron Letters* **1966**, *7*, 4533-5.
[19] J. A. Blake, E. Gagnon, M. Lukeman, J. C. Scaiano, *Organic Letters* **2006**, *8*, 1057-60.
[20] J.-M. Mewes, E. Pepler, J. Wachtveitl, A. Dreuw, *The Journal of Physical Chemistry A* **2012**, *116*, 11846-62.
[21] T. Guzzo, W. Mandaliti, R. Nepravishta, A. Aramini, E. Bodo, I. Daidone, M. Allegretti, A. Topai, M. Paci, *The Journal of Physical Chemistry B* **2016**, *120*, 10668-78.
[22] J.-D. Xiao, Q. Shang, Y. Xiong, Q. Zhang, Y. Luo, S.-H. Yu, H.-L. Jiang, *Angewandte Chemie International Edition* **2016**, *55*, 9389-93.
[23] A. Wang, Y. Zhou, Z. Wang, M. Chen, L. Sun, X. Liu, *RSC Advances* **2016**, *6*, 3671-9.

[24] J. B. DeCoste, G. W. Peterson, H. Jasuja, T. G. Glover, Y.-g. Huang, K. S. Walton, *Journal of Materials Chemistry A* **2013**, *1*, 5642-50.

[25] J. H. Cavka, S. Jakobsen, U. Olsbye, N. Guillou, C. Lamberti, S. Bordiga, K. P. Lillerud, *Journal of the American Chemical Society* **2008**, *130*, 13850-1.

[26] S. H. Jhung, J. H. Lee, J. W. Yoon, C. Serre, G. Férey, J. S. Chang, *Advanced Materials* **2007**, *19*, 121-4.

[27] K. M. L. Taylor-Pashow, J. Della Rocca, Z. Xie, S. Tran, W. Lin, *Journal of the American Chemical Society* **2009**, *131*, 14261-3.

[28] G. Férey, C. Mellot-Draznieks, C. Serre, F. Millange, J. Dutour, S. Surblé, I. Margiolaki, *Science* **2005**, *309*, 2040-2.

[29] M. Dan-Hardi, C. Serre, T. Frot, L. Rozes, G. Maurin, C. Sanchez, G. Férey, *Journal of the American Chemical Society* **2009**, *131*, 10857-9.

[30] A. De Vos, K. Hendrickx, P. Van Der Voort, V. Van Speybroeck, K. Lejaeghere, *Chemistry of Materials* **2017**, *29*, 3006-19.

[31] C. L. Hobday, C. H. Woodall, M. J. Lennox, M. Frost, K. Kamenev, T. Düren, C. A. Morrison, S. A. Moggach, *Nature Communications* **2018**, *9*, 1429.

[32] K. S. Park, Z. Ni, A. P. Côté, J. Y. Choi, R. Huang, F. J. Uribe-Romo, H. K. Chae, M. O'Keeffe, O. M. Yaghi, *Proceedings of the National Academy of Sciences* **2006**, *103*, 10186-91.

[33] L. B. d. Bourg, A. U. Ortiz, A. Boutin, F.-X. Coudert, *APL Materials* **2014**, *2*, 124110.

[34] L.-J. Li, P.-Q. Liao, C.-T. He, Y.-S. Wei, H.-L. Zhou, J.-M. Lin, X.-Y. Li, J.-P. Zhang, *Journal of Materials Chemistry A* **2015**, *3*, 21849-55.

[35] S. Devautour-Vinot, G. Maurin, C. Serre, P. Horcajada, D. Paula da Cunha, V. Guillerm, E. de Souza Costa, F. Taulelle, C. Martineau, *Chemistry of Materials* **2012**, *24*, 2168-77.